https://ntrs.nasa.gov/search.jsp?R=20200002626 2020-05-24T04:39:49+00:00Z

Quadrupole Simulations of Thermographic Inspections of Impacted Composites

William P. Winfree[a], Joseph N. Zalameda[b], and Patricia A. Howell[b]

[a]NASA Langley Research Center, MS 225, Hampton, Va, USA
[b]NASA Langley Research Center, MS 231, Hampton, Va, USA

ABSTRACT

Thermography has been shown to be a viable technique for inspection of composites. Impact damage in composites typically contains multiple overlapping delaminations at different depths. Understanding the limitations of the thermographic inspection is enhanced by performing simulations of the technique. Most simulations of composite thermographic inspections have focused on simulations of a single delamination at a fixed depth. The quadrupole method has been shown as a viable technique for rapid three-dimensional thermographic simulations of a delamination. This method is expanded to enable rapid simulation of multiple overlapping delaminations at different depths. Quadrupole simulations are compared to finite element simulations of multiple delaminations at different depths. The simulations are also compared to the thermographic measurements on impacted composites where shape and depth of the delaminations are known from x-ray computed tomography data.

Keywords: nondestructive evaluation, thermography, composite, simulation

1. INTRODUCTION

Flash thermography is an effective method for rapid inspection of large carbon fiber reinforced polymer (CFRP) composite structures. Simulations assist in developing an understanding of the limitations of the technique and enable quantitative characterization of subsurface flaws. Limited analytical or series solutions exist for heat diffusion in a solid and only for simple geometries.[?] Numerical techniques such as finite difference and finite element methods are well suited for such problems,[?,?] but can be computationally intensive. Both commercial[?,?,?,?] and noncommercial[?,?] simulation packages have successfully simulated thermographic nondestructive evaluations. For simulation of flash heating, some care is required, since the application of short duration flux to the surface results in large spatial temperature gradients near the surface at early times. To accurately simulate the thermal response, it is necessary to have closely spaced elements near the surface and/or start the simulation with an initial condition that assumes the flux was applied at a fixed time before the start of the simulation, rather than using Neumann boundary conditions to represent a short flux pulse.

Rather than simulating flash thermography in the time domain with finite element or finite difference techniques, it is possible to use the Laplace transform of the heat equation,[?] then invert the Laplace transform to produce a time domain response. For a limited number of configurations,it is possible to analytically invert the Laplace transform, however, common practice is to numerically perform the inversion. This is a very powerful technique when no analytic solution exists. It is often much faster and more accurate than finite difference or finite element techniques for the same configurations, since it is possible to solve for only the times of interest, there are fewer degrees of freedom for the same fidelity and the Laplace transform of impulse flux at the surface is a constant.

This is commonly referred to as the thermal quadrupole method, and is applicable for modeling heat diffusion in materials and structures in general[?] as well as flash thermography. For flash thermography, it has been used extensively for simulating the thermal response of multilayer systems with and without contact resistances at the

Further author information: (Send correspondence to W.P.W.)
W.P.W.: E-mail: william.p.winfree@nasa.gov, Telephone: +1 756 864 4962
J.N.Z.: E-mail: joseph.n.zalameda@nasa.gov, Telephone: +1 757 864 4793
P.A.H.: E-mail: p.a.howell@nasa.gov, Telephone: +1 757 864 4786

interfaces.[?,?,?,?,?,?,?] It has also been shown to be applicable for three-dimensional configurations, in particular for a delamination in CFRP composites[?,?,?,?] by representing the temperature as a cosine series and formulating the problem in terms of the Laplace transform of the coefficients.

This paper extends the three-dimensional quadrupole method to enable simulations of multiple delaminations at different depths, such as those resulting from impacts in CFRP composites. The location, shapes and contact resistance of impact induced delaminations in a composite are estimated from x-ray computed tomography data. This information is used as input into a quadrupole simulation and the results are compared to the measured thermographic response. There is reasonable agreement for early times. However, at later response times, the measured shapes of the delaminations are not as well delineated as they are in the simulated response. It is speculated that this is a result of contact resistance not being linearly dependent on the computed tomography estimation of delamination gap width.

2. QUADRUPOLE METHOD OF SIMULATING THERMAL RESPONSE OF LAYERS

A typical application of the quadrupole method is solving the one-dimensional heat equation of multilayer systems. For one-dimensional problems, a matrix is used to represent the relationship between the temperature and flux of one surface of the layer to the temperature and flux at the other surface (see Fig. 1). If two of the quantities are known (typically the fluxes at the surfaces), then it is possible to solve for the other two. The next subsection illustrates quadrupole method in one dimension. This facilitates understanding of the extension of the technique to three dimensions.

2.1 Quadrupole Method in One Dimension for Two Layers

A one-dimensional solution for the Laplace transform of temperature in an homogeneous material is[?]

$$v(z,s) = v(0,s)\cosh\left(z\sqrt{\frac{s}{\kappa}}\right) - f(0,s)\frac{\sinh\left(z\sqrt{\frac{s}{\kappa}}\right)}{K\sqrt{\frac{s}{\kappa}}}. \tag{1}$$

where K and κ are the thermal conductivity and diffusivity, respectively, $v(0,s)$ and $f(0,s)$ are the Laplace transform of temperature and flux at a point, s is the complex frequency variable and z is the vertical position. A similar expression for the Laplace transform of the flux as a function of position is

$$f(z,s) = f(0,s)\cosh\left(z\sqrt{\frac{s}{\kappa}}\right) - v(0,s)\sinh\left(z\sqrt{\frac{s}{\kappa}}\right)K\sqrt{\frac{s}{\kappa}}. \tag{2}$$

A simple way to express both of the equations is with the matrix formula

$$\begin{bmatrix} \cosh(q\ z) & -\frac{\sinh(q\ z)}{Kq} \\ -Kq\sinh(q\ z) & \cosh(q\ z) \end{bmatrix} \begin{bmatrix} v(0,s) \\ f(0,s) \end{bmatrix} = \begin{bmatrix} v(z,s) \\ f(z,s) \end{bmatrix}, \tag{3}$$

where $q = \sqrt{\frac{s}{\kappa}}$. From this matrix equation, the Laplace transform of either the temperatures ($v(0,s)$ and ($v(z,s)$) or fluxes ($f(0,s)$ and ($f(z,s)$) can be derived if any two of these is known. For example, for a plate with a thickness of d, if the fluxes at both surfaces are known, the temperatures are given by

$$v(0,s) = \frac{f(0,s)\coth(q\ d) - f(d,s)\mathrm{csch}(q\ d)}{Kq} \tag{4}$$

and

$$v(d,s) = \frac{\mathrm{csch}(q\ d)f(0,s) - f(d,s)\coth(q\ d))}{Kq}. \tag{5}$$

To find the temperature for the one-dimensional configuration shown in Fig. 1, first, solve for the temperature $v^+(d_1,s)$ above the interface at d_1 in terms of $f(0,s)$ and $f(d_1,s)$ using Eq. 5 and the temperature $v^-(d_1,s)$ below the interface in terms of $f(d_1,s)$ and $f(d_2,s)$ using Eq. 4. The difference between $v^+(d_1,s)$ and $v^-(d_1,s)$

is the flux times the thermal contact resistance (R) and the three equations, which need to be simultaneously solved are:

$$v^+(d_1,s) = v^-(d_1,s) + R * f(d_1,s), \tag{6}$$

$$v^+(d_1,s) = \frac{\text{csch}(q\ d_1) f(0,s) - f(d_1,s)\cosh(q\ d_1))}{Kq} \tag{7}$$

and

$$v^-(d_1,s) = \frac{f(d_1,s)\coth(q\ d_1) - f(d_2,s)\text{csch}(q\ d_2)}{Kq}. \tag{8}$$

By substituting $v^+(d_1,s)$ from Eq. 7 and $v^-(d_1,s)$ from Eq. 8 into Eq. 6, it is possible to solve for $f(d_1,s)$. Once $f(d_1,s)$ is found, it is possible to solve for both $v(0,s)$ and $v(d_1+d_2,s)$.

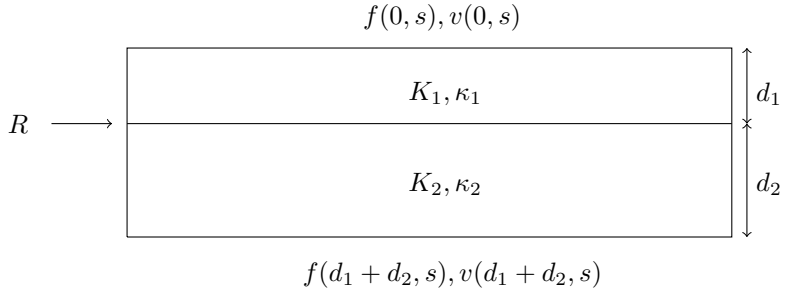

Figure 1: One dimensional configuration for a two layer system with a contact resistance between the two layers.

This is normally done more quickly by using

$$\begin{bmatrix} \cosh(q\ d_2) & \frac{-\sinh(q\ d_2)}{K_2 q} \\ -Kq\sinh(q\ d_2) & \cosh(q\ d_2) \end{bmatrix} \begin{bmatrix} 1 & -R \\ 0 & 1 \end{bmatrix} \begin{bmatrix} \cosh(q\ d_1) & \frac{-\sinh(q\ d_1)}{K_1 q} \\ -Kq\sinh(q\ d_1) & \cosh(q\ d_1) \end{bmatrix} \begin{bmatrix} v(0,s) \\ f(0,s) \end{bmatrix} = \begin{bmatrix} v(d_1+d_2,s) \\ f(d_1+d_2,s) \end{bmatrix}, \tag{9}$$

where the left most matrix corresponds to a transfer matrix for the lower layer, the center matrix is a transfer matrix corresponding to the boundary condition between the two layers and the right most matrix is the transfer matrix for the upper layer in Fig. 1. This results in two simultaneous equations and a solution for $v(0,s)$ and $v(d_1+d_2,s)$, which is equivalent to the solution found by combining Eqs. 6, 7 and 8. However, solving initially for the interface flux ($f(d_1,s)$) is similar to the approach that will be used for the multidimensional case. To find the temperature at a given time, the Laplace transform is normally numerically inverted.

The thermal response of multiple layers can be found by using this matrix formulation and is discussed in detail elsewhere.[?]

2.2 Quadrupole Method in Three Dimensions for Multiple Layers

Solving for the temperature in a stack of layers is performed following the same methodology discussed for the one-dimensional solution. First, equations relating temperature for the upper and the lower surface of a layer to the flux on the upper and lower surface of the layer are derived. As was done for the one-dimensional case, the solutions are derived for the Laplace transform of the temperature at each point. For any given $x-y$ plane, it is useful to define the Laplace transform of temperature and flux in the $x-y$ plane as a cosine transform. This representation requires that the no heat flow across the four sides of the stack. The two-dimensional cosine transform of temperature is given by

$$v(x,y,z,s) = \sum_{m=0}^{M-1}\sum_{n=0}^{N-1} a_m a_n \tilde{v}_{m,n}(z,s)\cos\left(\frac{\pi m x}{L_x}\right)\cos\left(\frac{\pi n y}{L_y}\right), \tag{10}$$

where $a_m = 1$ if m is equal to 0 or $M-1$, otherwise $a_m = 2$ and the cosine series coefficient is $\tilde{v}_{m,n}(z,s)$ is given by

$$\tilde{v}_{m,n}(z,s) = \frac{\sum_{i=0}^{M-1}\sum_{j=0}^{N-1} a_i a_j v(x_i, y_j, z, s) \cos\left(\frac{\pi m x_i}{L_x}\right) \cos\left(\frac{\pi n y_j}{L_y}\right)}{(2M-2)(2N-2)} \tag{11}$$

or when the temperature is defined at a set of M by N for evenly spaced locations given by $x_m = mL_x/(M-1)$ and $y_n = nL_y/(N-1)$,

$$\tilde{v}_{m,n}(z,s) = \frac{\sum_{i=0}^{M-1}\sum_{j=0}^{N-1} a_i a_j v_{i,j}(z,s) \cos\left(\frac{\pi i m}{M-1}\right) \cos\left(\frac{\pi j n}{N-1}\right)}{(2M-2)(2N-2)}. \tag{12}$$

The flux in the layer at the same x and y locations is given by a similar expression

$$f_{m,n}(z,s) = \frac{\sum_{i=0}^{M-1}\sum_{j=0}^{N-1} a_m a_n \tilde{f}_{i,j}(z,s) \cos\left(\frac{\pi i m}{2M-2}\right) \cos\left(\frac{\pi j n}{2N-2}\right)}{(2M-2)(2N-2)}, \tag{13}$$

where $\tilde{f}_{m,n}(z,s)$ is also given by Eq. (12), if f is substituted for v. Within a layer, Eq. (10) is a solution to the Laplace transform of the heat equation if the cosine series coefficients have a z dependence given by an expression similar to Eq. 1:

$$\tilde{v}_{m,n}(z,s) = \tilde{v}_{m.n}(0,s)\cosh\left(q_{m,n}\ z\right) - \tilde{f}_{m,n}(0,s)\frac{\sinh\left(q_{m,n}\ z\right)}{K q_{m,n}}, \tag{14}$$

where $q_{m,n}$ is given by

$$q_{m,n} = \sqrt{\frac{s}{\kappa_z} + \frac{\kappa_x}{\kappa_z}\left(\frac{\pi m}{L_x}\right)^2 + \frac{\kappa_y}{\kappa_z}\left(\frac{\pi n}{L_y}\right)^2}. \tag{15}$$

This is similar to the one-dimensional equation for the z dependence of the Laplace transform (Eq. (1)) and the z dependence of flux similar to Eq. (2). Within a layer, there is a simple matrix equation similar to Eq. (3) for each spatial frequency coefficient in Eq. (12),

$$\begin{bmatrix} \cosh\left((z_2-z_1)q_{m,n}\right) & -\frac{\sinh((z_2-z_1)q_{m,n})}{K q_{m,n}} \\ -K q_{m,n}\sinh\left((z_2-z_1)q_{m,n}\right) & \cosh\left((z_2-z_1)q_{m,n}\right) \end{bmatrix} \begin{bmatrix} \tilde{v}_{m,n}(z_1,s) \\ \tilde{f}_{m,n}(z_1,s) \end{bmatrix} = \begin{bmatrix} \tilde{v}_{m,n}(z_2,s) \\ \tilde{f}_{m,n}(z_2,s) \end{bmatrix}. \tag{16}$$

It can be shown that for any layer in the stack the temperature of the top and bottom of a layer can be expressed in terms of the flux at the top and bottom of the layer by

$$\mathbf{v}(p_n,s) = \mathbf{C}^{\coth}(d_n,s)\cdot\mathbf{F}(p_n,s) - \mathbf{C}^{\mathrm{csch}}(d_n,s)\cdot\mathbf{F}(p_{n+1}) \tag{17}$$

and

$$\mathbf{v}(p_{n+1},s) = \mathbf{C}^{\mathrm{ccsh}}(d_n,s)\cdot\mathbf{F}(p_n,s) - \mathbf{C}^{\coth}(d_n,s)\cdot\mathbf{F}(p_{n+1}) \tag{18}$$

where p_n and p_{n+1} are the z locations of the top and bottom of the layer, d_n is the layer thickness, $\mathbf{v}(z,s)$ and $\mathbf{F}(z,s)$ are matrices representing the temperature and flux at z, and $\mathbf{C}_{\cosh}(d_n,s)$ and $\mathbf{C}_{\mathrm{csch}}(d_n,s)$ are matrices with elements given by

$$C^{\coth}_{i,j,m,n}(d,s) = a_m a_n \frac{\sum_{p=0}^{M-1}\sum_{q=0}^{N-1} a_p a_p \cos\left(\frac{ip\pi}{M-1}\right)\cos\left(\frac{mp\pi}{M-1}\right)\cos\left(\frac{jq\pi}{N-1}\right)\cos\left(\frac{nq\pi}{N-1}\right)\coth(q_{m,n}d)}{(2M-2)(2N-2)}, \tag{19}$$

and

$$C^{\mathrm{csch}}_{i,j,m,n}(d,s) = a_m a_n \frac{\sum_{p=0}^{M-1}\sum_{q=0}^{N-1} a_p a_p \cos\left(\frac{ip\pi}{M-1}\right)\cos\left(\frac{mp\pi}{M-1}\right)\cos\left(\frac{jq\pi}{N-1}\right)\cos\left(\frac{nq\pi}{N-1}\right)\mathrm{csch}(q_{m,n}d)}{(2M-2)(2N-2)}, \tag{20}$$

To find the temperature at the front surface from Eq. 17, since $\mathbf{F}(p_0, s)$ is a given, it is necessary to find $\mathbf{F}(p_1, s)$. This requires finding the flux at all the interior interfaces. At any interface, the flux is related to flux at the adjacent interface by boundary conditions at the interface. At the interface between layers n and $n+1$, the temperature above interface ($\mathbf{v}^+(p_{n+1}, d)$) and the temperature below the interface ($\mathbf{v}^-(p_{n+1}, d)$) are given by

$$\mathbf{v}^+(p_{n+1}, s) = \mathbf{C}^{\text{ccsh}}(d_n, s) \cdot \mathbf{F}(p_n, s) - \mathbf{C}^{\text{coth}}(d_n, s) \cdot \mathbf{F}(p_{n+1}, s) \tag{21}$$

and

$$\mathbf{v}^-(p_{n+1}, s) = \mathbf{C}^{\text{coth}}(d_{n+1}, s) \cdot \mathbf{F}(p_n + 1, s) - \mathbf{C}^{\text{csch}}(d_{n+1}, s) \cdot \mathbf{F}(p_{n+2}, s). \tag{22}$$

The temperature across the interface with a spatially varying contact resistance given by $R(x, y)$ is

$$\mathbf{v}^-(p_n, s) = \mathbf{v}^-(p_{n+1}, s) + \mathbf{R} \cdot \mathbf{F}(p_n + 1, s) \tag{23}$$

where $\mathbf{R}$ has elements $R_{i,j,m,n}$ which are $R(x_i, y_j)$ if $i = m$ and $j = n$ and zero otherwise.

It is possible to find all of the interior interface fluxes from a large number of simultaneous equations based on Eqs. 22-23, however, it is computationally simpler to solve for fluxes iteratively. This is performed by estimating the flux at each interior interface with the one-dimensional solution. Starting with the interface closest to the surface of interest, the flux at that interface is updated based on the two adjacent fluxes. The updated flux is used to update the next flux at the next interface in the stack and the process is continued until all of the fluxes have been updated. The updated fluxes are then the starting point for another iteration of updates. To date, after one iteration, additional iterations result in value changes of less than 0.1%.

3. COMPARISON OF QUADRUPOLE METHOD AND FINITE ELEMENT SIMULATION RESULTS

A simulation of the configuration shown in Fig. 2 was performed with both the quadrupole and finite element methods. The lateral dimensions of the stack were set to 5 cm by 5 cm with a thickness of 0.2 cm, with each layer in the stack being 0.01 cm. Each of the circles represents a region of contact resistance at an interface between first six layers in the stack equivalent to 0.03 cm of air. These contact resistances do not add to the thickness of the stack. The radius of the smallest circle closest to the surface was 0.25 cm and the radius increases by 0.25 cm for each subsequent depth. The right edge of all the circles are aligned. The material properties were a thermal conductivity of 0.97 W/°K/m, a heat capacity of 1269 J/°K/M and a density of 1490 Kg/m^3. For these properties, the thermal diffusivity of the layer is 0.005 cm^2/sec, which is a reasonable approximation for a CFRP composite.

(a) (b)

Figure 2: Three-dimensional configuration for a block with five circular regions of high contact resistance at five different depths. (a) A view from the side of the block showing the regions of high contact resistance are at multiple depths in the block. (b) A view from the top of the block indicating how the regions of high contact resistance are overlapped.

Comparison of results obtained from the quadrupole and finite element simulations are shown in Fig. 3. The results for all times appear very similar visually. For each time, the images have been scaled to the minimum and maximum values of the image pairs. Differences between the two simulations are more easily visualized in Fig. 4. The temperatures in the plots are normalized such that the value has a limit of one for long times. A comparison of spatial profiles across the vertical centers of the configuration are shown in Fig. 4a. As can be seen from the figure, the agreement is better at later times than at early times. The shapes of the profiles are all approximately the same. The largest difference between the two simulations is less than 2%.

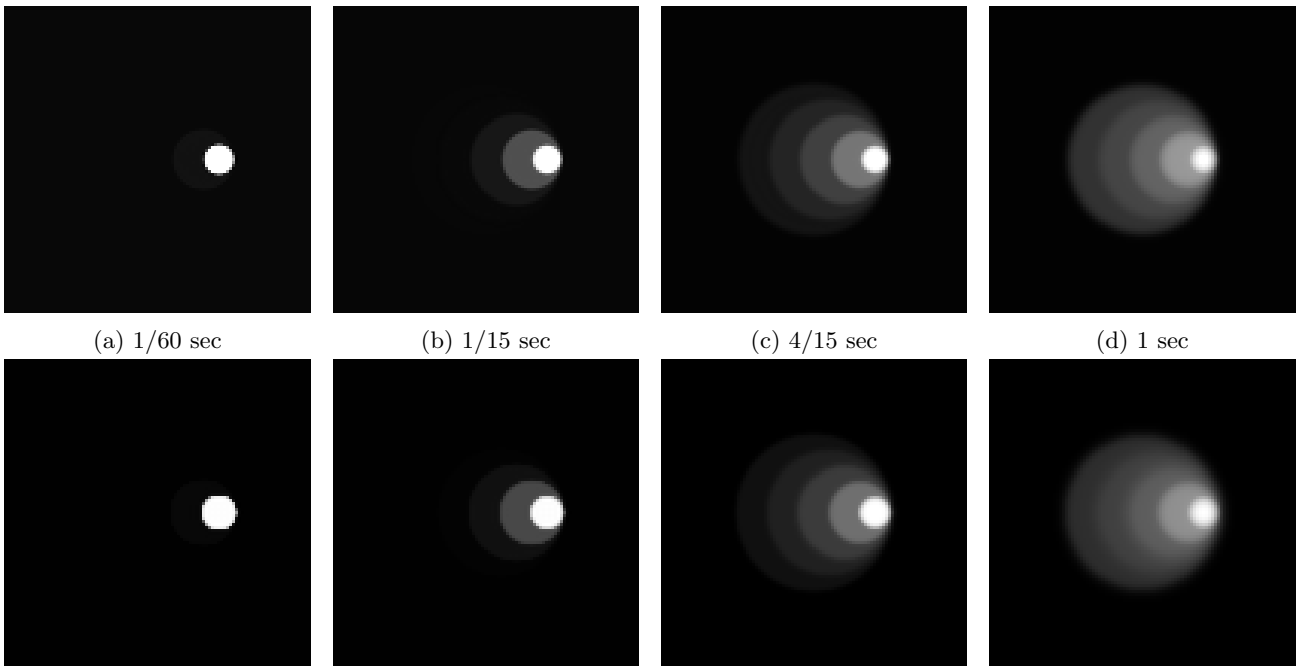

(a) 1/60 sec (b) 1/15 sec (c) 4/15 sec (d) 1 sec

(e) 1/60 sec (f) 1/15 sec (g) 4/15 sec (h) 1 sec

Figure 3: A comparison of the finite element and quadrupole simulations of the configuration shown in Fig. 2 with five circular regions of high contact resistance at five different depths. (a-d) are images created from the finite element results at four different times and (e-h) are the corresponding images created from the quadrupole simulation. The times for each pairs appear in the subtitles.

The temporal responses at the locations 0.0 cm, 1.5 cm, 2.0 cm, 2.5 cm, 3.0 cm and 3.5 cm are shown in Fig. 4b. The first of these corresponds to a location with no contact resistance beneath it, the next five having the first contact resistance at 0.05 cm, 0.04 cm, 0.03 cm, 0.02 cm and 0.01 cm beneath the surface. The most notable characteristics of these temporal responses are the largest differences occur at early times and better agreement occurs for deeper contact resistances.

4. ESTIMATION OF THE CHARACTERISTICS OF IMPACT INDUCED DELAMINATIONS IN A CFRP COMPOSITE

Both thermography and x-ray computed tomography data were acquired on an impacted CFRP composite. There is a clear indentation on the impacted surface and the opposite surface has a slight bulge. The lateral dimensions of the composite are approximately 6.8 cm by 3.8 cm and it is approximately 0.32 cm thick. The thermography response was measured on the surface with a bulge.

A computed tomography cross section of a portion of the impacted composite is shown in Fig. 5. The voxel size of the computed tomography data is 40 μm on a side. The region shown in the image is 1.200 cm by 0.344 cm. The top of the image contains the data that is closest to the thermographic response surface. As can be

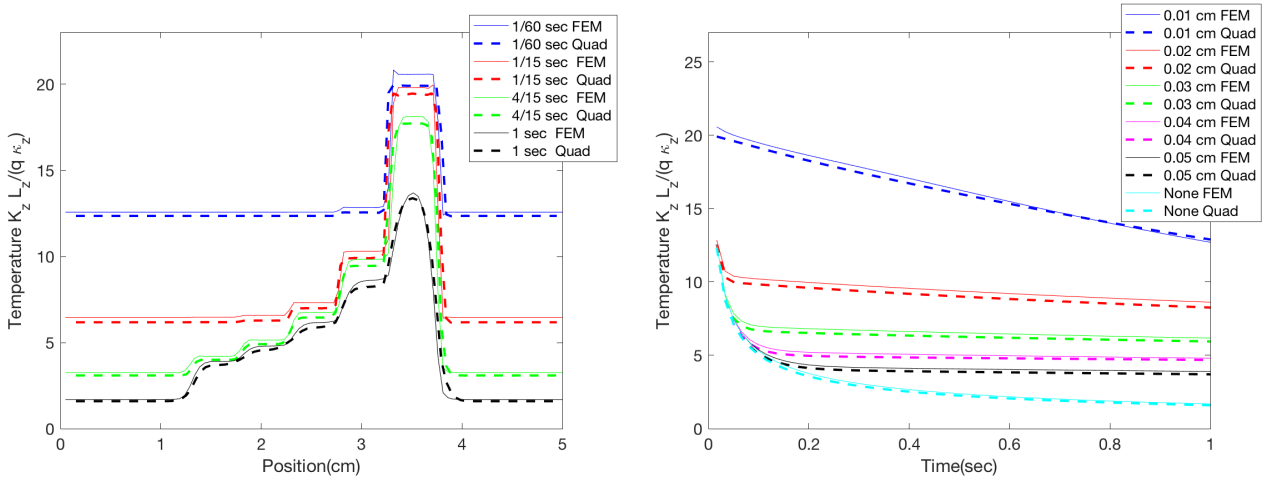

(a) (b)

Figure 4: (a) The temperature profile across the vertical center of the simulations for the configuration shown in Fig. 2. (b) The temperature as a function of time for each of the different depths of contact resistance.

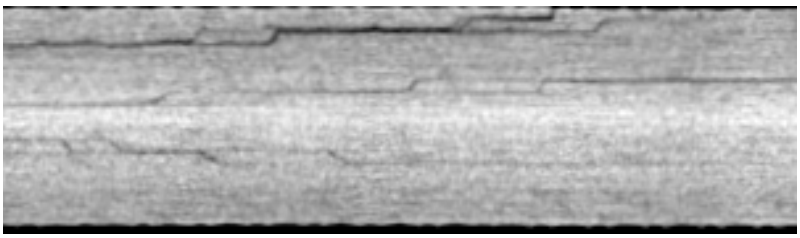

Figure 5: A slice from the x-ray computed tomography data clearly shows the delaminations at different depths in the composite.

seen from the image, not all of the delaminations have the same gap width. In this image, the delaminations at the top of the slice clearly have wider gaps than those deeper in the slice.

From the computed tomography data, it appears that there are delaminations at thirteen interfaces. Most of the interfaces have two significant delaminations. A three-dimensional representation of these delaminations is shown in Fig. 6a. The volume shown is 3.2 cm by 3.2 cm by 0.332 cm. The vertical aspect is 8 times the in-plane aspect for improved visualization of the delaminations. Each color represents a different depth. Shown with the three-dimensional view is a view (Fig. 6b), form the perspective above the thermography response surface.

For each of the interfaces, a gap width map was generated from the the computed tomography data. This process involved both a manual outlining of the delaminations, then a determination of the ct number in the outlined region. The gaps of the delamination were estimated from the reduction in the ct number in the region of the delamination, an estimation of the point spread function from the computed tomography data at the edge of the composite and an estimate of the nominal ct number of the composite. For points with ct numbers greater than the nominal ct number of the composite, the gap width was set to zero. The computed tomography data from the first, second, third, fifth and sixth interfaces are shown with the associated thickness map in Fig. 7. Interface numbers were found by dividing the depth of the indication by ply thickness, then rounding to the nearest number. All of the images are scaled the same and the region shown in each image is 3.2 cm by 3.2 cm. As can be seen in the figure, the first two interfaces (Fig. 7a and Fig. 7b), have regions that are much darker than any indication in the fifth interface(Fig. 7d). This indicates these delaminations have wider gaps than the other interfaces, as was mentioned in the discussion of Fig. 5. All of the thickness maps are scaled from 0 to 50 μm. The gap thickness maps are used to estimate the contact resistance of the delaminations at each interface.

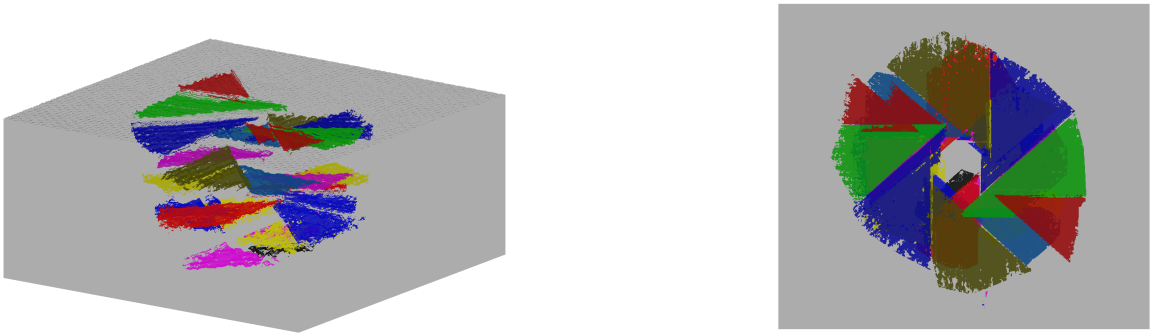

(a) (b)

Figure 6: Three-dimensional representation of the computed tomography data. (a) View of the data from the side. (b) The same data view from the above the surface of the thermography characterization.

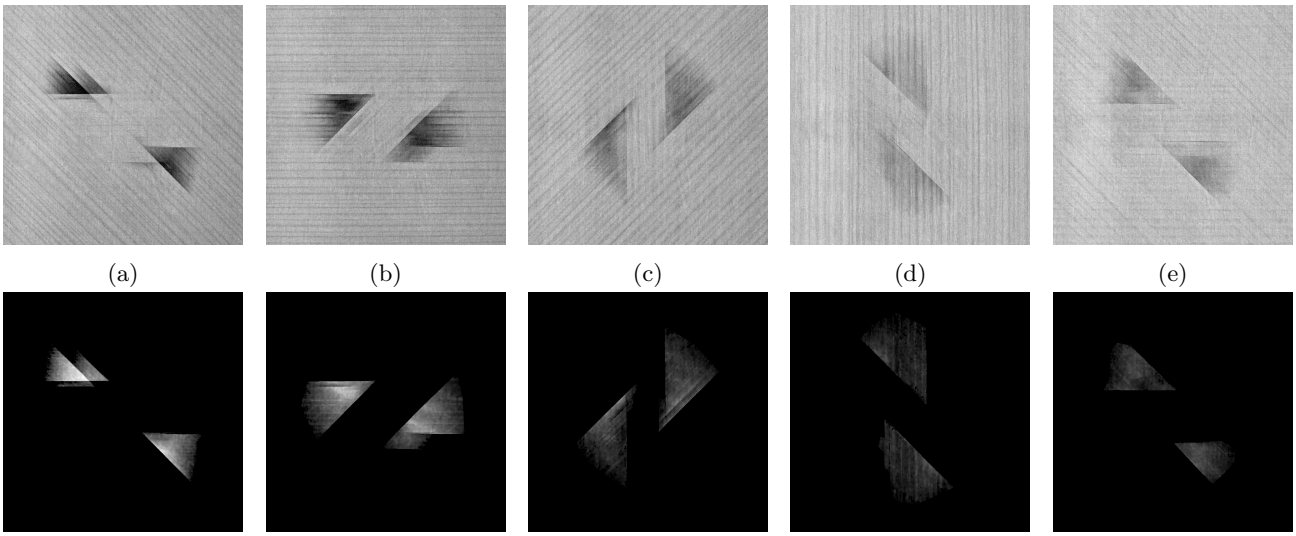

(a) (b) (c) (d) (e)

(f) (g) (h) (i) (j)

Figure 7: (a-e) are computed tomography images of the subsurface delaminations. From left to right the locations of the delaminations are at the first, second, third, fifth and sixth interfaces below the thermographic characterization surface. (f-j) The gap thickness images, calculated for the above delaminations.

The size, maximum gap width and median gap width for each interface with a detected delamination are shown in Table 1. As can be seen from the table, the widest gap spacing occurs for the delaminations closest to the surface. This was also apparent in the computed tomography image shown in Fig. 5. Note that the delaminated area at interface three is almost twice the area as interface one.

Table 1: Depth, area and gap width of delaminations observed in computed tomography data.

Interface Number	Interface Depth	Delamination Area	Maximum Gap	Median Gap
1	0.0178 cm	0.494 cm^2	50 μm	21 μm
2	0.0347 cm	0.883 cm^2	41 μm	16 μm
3	0.0532 cm	0.979 cm^2	31 μm	9 μm
5	0.0902 cm	1.03 cm^2	21 μm	7 μm
6	0.1008 cm	0.598 cm^2	22 μm	9 μm
7	0.1264 cm	0.549 cm^2	22 μm	7 μm
9	0.1435 cm	0.586 cm^2	20 μm	16 μm
10	0.1797 cm	0.800 cm^2	27 μm	7 μm
11	0.1971 cm	0.417 cm^2	29 μm	6 μm
12	0.2155 cm	0.719 cm^2	27 μm	6 μm
13	0.2338 cm	0.636 cm^2	25 μm	6 μm
15	0.2701 cm	0.421 cm^2	24 μm	7 μm
16	0.2863 cm	0.062 cm^2	20 μm	6 μm

5. COMPARISON OF QUADRUPOLE ESTIMATION OF THERMOGRAPHIC AND MEASURED THERMOGRAPHIC RESPONSE

The thickness maps, such as shown in Fig. 7, are divided by the thermal conductivity of air (2624. Erg/cm/°K/sec) to create contact resistance maps. For the simulations, layer thicknesses are set to the change in depth between interfaces where delaminations are detected.

For the simulation, the input material properties were thermal conductivity of 0.97 W/°K/m and surface normal and in-plane thermal diffusivity of 0.005 cm^2/sec. This is a reasonable approximation for CFRP composites based on previous measurements. A comparison of the result of the quadrupole simulation and the measured thermographic response at four different times are shown in Fig. 8. The resolution of the thermographic data is 0.025 cm and the resolution in the simulations is slightly better, 0.017 cm. The size of the thermographic data and the simulations is 1.7 cm by 1.7 cm. For the experimental data, the first time after the flash with a clear thermographic response is 0.1 sec.

As can be seen from Fig. 8, there is reasonable agreement for early times, 0.2 sec and less. For these times, the simulation and experimental data have approximately the same contrast between delaminated and sound material. The shapes of the indications are also approximately the same. For later times, the agreement is not as good. Based on an examination of the gap thickness maps, it appears disagreement at later times is greatest in regions with the smallest gap thickness.

Two simple approaches were attempted to improve the agreement between the simulation and measurement. The first was to increase the in-plane diffusivity to 0.05 cm^2/sec. This value is at the upper limit of what is expected for the in-plane diffusivity in CFRP composites. This resulted in a blurring of the shapes at later times, however, it did not significantly change the shapes of delaminations. The second approach was assuming the gap thickness measurement resulted in a gap thickness that was too large. Reducing the gap spacing by a factor of two also did not result in a significant change in the shape of the indications at latter times.

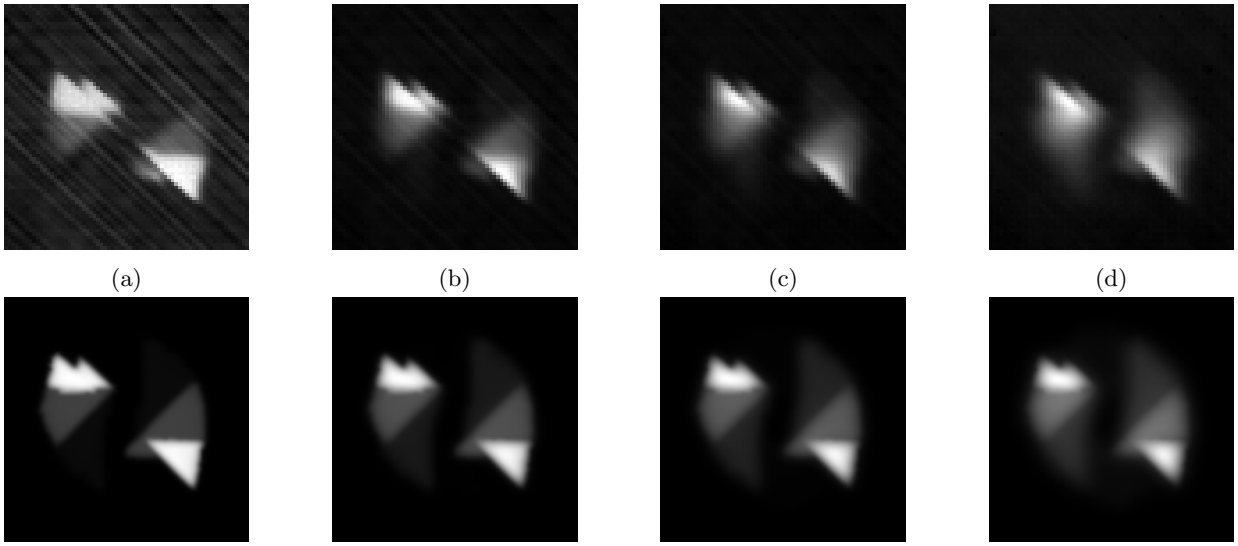

Figure 8: (a-d) Measured thermographic response from left to right, 0.1 sec, 0.2 sec, 0.3 sec and 0.5 sec after flash heating. (e-h) Simulated thermographic responses for the same times as (a-d)

A comparison of the gap thickness maps in Fig. 7 and the later times in Fig. 8 indicate the indications decrease faster in the regions with smaller gaps. A possible explanation could be there is not a linear relationship between the contact resistance and the gap width. An examination of the surface of the delamination indicates that it is rough. For very small gaps, the surfaces may be intermittently in contact, which reduces the contact resistance. As the gap gets larger, it is expected there is less contact. For this situation, the contact resistant would not be linearly dependent on the average width of the gap. Future efforts will use the quadrupole simulation to explore this possibility.

6. CONCLUSION

A methodology has been developed for incorporation of regions of significant contact resistance at multiple depths into a three-dimensional quadrupole simulation of the thermal response of a stack of layers. The method involves calculation of the fluxes at interior interfaces from the adjacent interface fluxes. The results of the method were compared to the simulation results obtained from finite element simulation on the same configuration. The thermal properties were chosen to be approximately the same as those found in a CFRP composite. The agreement between to two was within 2%.

The methodology was also applied to simulation of an impacted CFRP composite. The multiple delaminations of the composite were characterized using computed tomography data. From the computed tomography data, the delamination sizes, depths and gap widths were estimated. This information was input into the quadrupole simulations. Reasonable agreement between experimental data and simulation was found for early times (less than 0.2 sec). For longer times, indications above regions with small gap spacings tend to fade faster than what is seen in the simulation. It is speculated that the contact resistance in these region is reduced by intermittent contact between the two surfaces of the delamination.